Transport phenomena in high porosity metal foams

Roop L. Mahajan   *mahajan@spot.colorado.edu*
Department of Mechanical Engineering
University of Colorado at Boulder, Boulder, CO 80309-0427

Abstract. *High porosity metal foams are potentially excellent candidates for high heat dissipation. These metal foams have porosities of around 90% and are available in different pore sizes characterized by PPI (pores per inch). They not only provide extended surface area but also serve to enhance the convective heat transfer due to local thermal dispersion caused by the eddies that are shed in the wake of the flow past the metal fibers. The attendant penalty is in high-pressure drop due to the extra resistance offered by the tortuous flow paths of the cooling medium.*

Most of the reported work related to transport phenomena in porous media relates to low porosity materials. Not much is known about the convective or two phase flows in high porosity metal foams. Over the last seven years, we have conducted research to fill the knowledge gap in this field. The important findings will be discussed in this talk.

First, both the analytical relations and experimental data for the effective thermal conductivity of such porous media will be presented. We have shown that the effective thermal conductivity for these foams lies in between the upper and the lower limit given by the parallel and series arrangement, respectively. For convective transport, a volume-averaged approach is used to derive the governing Navier-Stokes and energy equations. In the latter, the assumption of local thermal equilibrium is relaxed and two separate equations, one for the fluid and the other for the matrix material, are derived. The equations are numerically solved for both buoyancy-induced and forced convection flows. Complimented by the experimental data, the coefficient of thermal dispersion is determined and results of parametric study are presented to understand the heat transfer results as a function of the relevant non-dimensional parameters.

The paper will also present our results on "pool" boiling of Fluorinert fluids in such foams. The experimental data reveals interesting features. The overshoot at the transition from natural convection to nucleate boiling is absent and the transition from nucleate to film boiling is smooth. These results have strong implications for electronic cooling applications.

Keywords: porous media, metal foams, transport, convection, boiling

Nomenclature

A   surface area of metal foam (m^2)

a_{sf} specific solid-fluid interfacial surface area (m^{-1}) (Eq.(20))

Bi_f $= h_{sf}\, a_{sf}\, H\, \sqrt{K}\, / k_{fe}$, fluid-phase effective Biot number

Bi_s $= h_{sf}\, a_{sf}\, H^2\, k_{se}$, solid-phase effective Biot number

C_D coefficient of thermal dispersion (Eq.(21))

C_T coefficient in Eq.(19)

Da $= \sqrt{K}/H$, Darcy number

f inertia coefficient

$\bar{h}$ average heat transfer coefficient from heated surface (W/m^2 - K)

h_{sf} interfacial heat transfer coefficient (W/m^2 - K)

H height of metal foam sample

k conductivity (W/m - K)

K permeability (m^2)

L length of heated section of metal foam

N number of fibers

Nu $= \bar{h}L/k_e$, measured and computed average Nusselt number

p volume-averaged pressure

Pr_e $= \mu c_p / k_e$, Prandtl number based on effective conductivity

Pe $= Re_K Pr_e$, Peclet number

q heat input to patch heaters (W)

Re_K $= u_o\, \sqrt{K}\, / v$, Reynolds number based on permeability

T volume-averaged temperature (°C)

T_{in} measured fluid temperature (before entering heated section) (°C)

T_{amb} measured fluid temperature (before entering unheated section) (°C)

T_{wi} measured wall temperatures (°C)

ΔT_{avg} average wall temperature with respect to fluid inlet temperature, T_{in}

u_o measured average flow velocity entering foam sample (m/s)

u x-velocity component (m/s)

u velocity vector

U $= u/u_o$, non-dimensional x-velocity component

x,y,z coordinates in the streamwise, transverse, lateral directions

X,Y $= x/H, y/H,$ non-dimensional coordinates

Greek symbols

ν kinematic viscosity

ε porosity

ρ density

θ $= (T - T_{in}) / (T_{avg})$

Subscripts

f fluid

s solid

d dispersive

e effective

x x-component

y y-component

1. Introduction

Convective transport in porous media has been studied extensively for over fifty years (see Kaviany (1991) for a good review on the subject). However, most studies in this category have been restricted to packed beds and granular materials. They have porosities in the range 0.4 - 0.6 and have direct applications to naturally occurring porous media. The subject matter of this paper is high porosity media ($\varepsilon > 0.9$), such as metal foams.

Figure 1 shows a picture of the metal foam medium. It has an open-celled structure composed of dodecahedron-like cells, which have 12-14 pentagonal or hexagonal faces. The edges of these cells are composed of the fibers and, typically, there is a lumping of material at points where the fibers intersect. The fibrous matrix is made of aluminum alloy T-6201 that has a thermal conductivity of 218 W/m-K. The matrix is brazed to aluminum base plates on two sides. Two quantities, the porosity and the pore density, are used to describe the material. The porosity, ε, is the ratio of the void volume to the total volume of the medium and the pore density is the number of pores present per unit length of the material. The latter is typically expressed in units of pores per inch (PPI), and is roughly constant in the three directions.

The geometry of a porous medium can be represented by its characteristic length. In classical porous media studies, the sphere or particle diameter can be used as a characteristic length, and the porosity of the matrix can be either calculated or measured. In metal foams, both porosity and the number of pores per unit length are measurable quantities. However, the pore diameter, which for the metal foam is the characteristic length of the space between the metal

strands, is unknown. To determine this, an open cell representation, as shown in Fig. 2, can be used to approximate the metal foam structure.

It is shaped as a cube of volume H^3, with porosity ε, with N fibers of diameter d_f and N pores of diameter d_p in each of the *x, y, z* directions. The total number of fibers in each direction is N^2. Thus, for a giving porosity ε, we can represent the total solid volume of the cube as:

$$3N^2 \times \frac{\pi d_f^2}{4} \times H = (1-\varepsilon) \times H^3 \tag{1}$$

Further, noting that:

$$\frac{N}{H} = PPI \ (or \ PPM) \ \text{and} \quad N(d_f + d_p) = H \tag{2}$$

we obtain an expression for the pore diameter:

$$d_p = \frac{1}{PPI \ (or \ PPM)} \left[1 - 2\sqrt{\frac{(1-\varepsilon)}{3\pi}} \right] \tag{3}$$

The pore diameter obtained is unique for each sample and can be used as the characteristic length, as it is a function of both the number of pores per unit length and the porosity of the material.

The published studies on transport phenomena in high porosity metal foams are relatively few, and more recent. In fact, at the time of our undertaking research on the topic, in 1992, the only directly relevant study was due to Hunt and Tien (1988), in which they had studied forced convection in metal foams with water as the fluid phase. Our work was motivated by the potential application of metal foams as heat sinks for meeting the high thermal dissipation requirements in electronic cooling, using air as the fluid phase. It was hypothesized that the extended surface area provided by the foam metal, coupled with thermal dispersion due to the locally shed eddies in the wake of the metal foam fibers, would lead to larger thermal dissipation than possible with the conventional heat sinks. To test this premise, Lee *et al*. [1993], conducted a preliminary experimental study and showed that in a ducted fan arrangement and using a low power muffin DC-fan, a 1 cm^2 chip dissipating 100 W could be cooled using a 6.35 cm × 6.35 cm × 2.54 cm high aluminum foam heat sink with a 40° temperature rise.

Encouraged by these results, a systematic numerical and experimental investigation was undertaken to reveal the underlying physics and to quantify the thermal performance of these heat sinks in forced and buoyancy-induced convection [Calmidi, 1998; Calmidi and Mahajan , 2000; Phanikumar and Mahajan, 2000)]. This research was supplemented by analytical and experimental studies of effective thermal conductivity of such foams [Calmidi and Mahajan (1999), Bhattacharya *et al.* (1999)]. To investigate the performance of these foams for high thermal dissipation, pool boiling experiments using a fluorinert fluid FC-72®, were also conducted (Arbelaez *et al*., 2000). What follows is a brief summary of these investigations.

2. **Forced Convection Transport**

The following governing continuity and momentum equations for the metal foams can be derived using the well-known volume averaged procedure for porous media (Whitaker, 1967; Vafai and Tien, 1981).

Continuity and Momentum:

$$\nabla \cdot \langle \mathbf{v} \rangle = 0 \tag{4}$$

$$\frac{\rho_f}{\varepsilon^2}\langle\mathbf{v}\rangle\cdot\nabla\langle\mathbf{v}\rangle = -\nabla\langle p\rangle^f + \frac{\mu}{\varepsilon}\nabla^2\langle\mathbf{v}\rangle - \frac{\mu}{K}\langle\mathbf{v}\rangle - \frac{C}{K^{1/2}}\rho_f|\langle\mathbf{v}\rangle|\langle\mathbf{v}\rangle \qquad (5)$$

In Eq. (5), the last three terms are the Brinkman (or friction) term, the Darcy term and the Forchheimer (or inertia) terms, respectively. The notation $< >$ is used to denote the local volume average of a quantity.

Energy transport in porous media is generally studied by invoking the assumption of local thermal equilibrium (LTE). The validity of this assumption for metal foams is doubtful in view of the vastly different thermal conductivities for the solid (generally Al) and fluid (air) combinations. As a result, the effects of local thermal non-equilibrium (LTNE) need to be included. To this end, a two-equation model (Amiri and Vafai, 1994; Amiri *et al.*, 1995; Jiang *et al.,* 1999; Nield and Kuznetson, 1999; Calmidi and Mahajan, 2000), is needed. The volume averaged solid phase and the fluid phase energy equations are:

Energy Equation for the Fluid:
$$\langle\rho_f\rangle^f c_{pf}\langle\mathbf{v}\rangle\cdot\nabla\langle T_f\rangle^f = \nabla\cdot\left\{(k_{fe}+k_d)\cdot\nabla\langle T_f\rangle^f\right\} + h_{sf}a_{sf}(\langle T_s\rangle^s - \langle T_f\rangle^f) \qquad (6)$$

Energy Equation for the Solid Matrix:
$$0 = \nabla\cdot\left\{k_{se}\cdot\nabla\langle T_s\rangle^s\right\} - h_{sf}a_{sf}(\langle T_s\rangle^s - \langle T_f\rangle^f) \qquad (7)$$

where the subscripts s and f denote solid and fluid phase, respectively. The fluid and solid phase effective thermal conductivities, k_{se} and k_{fe}, respectively, are functions of the structure of the medium and the individual conductivities k_s and k_f. The dispersion thermal conductivity, k_d, is used to account for the effect of pore-level hydrodynamics on the macroscopic transport. The term, $h_{sf}a_{sf}(<T>^s - <T>^f)$ is used to achieve the coupling between the two energy equations and represents the energy transferred between the two phases due to the temperature difference, where h_{sf} is the heat transfer coefficient that governs this phenomenon and a_{sf} is the specific solid-fluid interfacial area defined as the total interstitial surface area of the pores per unit bulk volume (Bear, 1972).

The quantities k_{se}, k_{fe}, K, f, k_d, h_{sf} and a_{sf} need to be determined before one can proceed to solve Eq. (4) to (7), subject to specific boundary conditions. The first five of these have to be determined experimentally; h_{sf} can be estimated from the correlations reported in the literature (Zhukauskas, 1972), and a_{sf} can be calculated based on the foam structure. A description of the evaluation of all of these quantities is given below.

2.1 Determining k_{se} and k_{fe}

Calmidi and Mahajan (1999) developed an analytic model for determining k_e, the effective thermal conductivity of metal foams. Assuming a periodic structure for the metal foam, see Fig. 3, they proposed a one-dimensional heat conduction model, considering the porous medium to be formed of a two-dimensional array of hexagonal cells. In commercially available metal foams, there is an irregular shaped lump of metal at the intersection of two fibers. This was represented as a square "blob" of metal at the intersection of two sides of a hexagon, Fig. 3. Since the structure assumed is periodic, the analysis was confined to a unit cell, Fig. 4. This unit cell was divided into three different layers in series and the effective thermal conductivity of each layer, in turn, was derived separately by treating the solid and fluid layers in parallel. The final

expression for the effective thermal conductivity was found to be

$$k_{eff} = \left[\left(\frac{2}{\sqrt{3}} \right) \left(\frac{r\left(\frac{b}{L}\right)}{k_f + \frac{(k_s - k_f)}{3}\left(1 + \frac{b}{L}\right)} + \frac{(1-r)\left(\frac{b}{L}\right)}{k_f + \frac{2}{3}(k_s - k_f)\left(\frac{b}{L}\right)} + \frac{\frac{\sqrt{3}}{2} - \frac{b}{L}}{k_f + \frac{4r}{3\sqrt{3}}(k_s - k_f)\left(\frac{b}{L}\right)} \right) \right]^{-1} \quad (8)$$

where

$$\frac{b}{L} = \frac{-r + \sqrt{r^2 + 4(1-\varepsilon)\frac{\sqrt{3}}{2}\left(\left(2 - r\left(1 + \frac{4}{\sqrt{3}}\right)\right)/3\right)}}{\frac{2}{3}\left(2 - r\left(1 + \frac{4}{\sqrt{3}}\right)\right)} \quad (9)$$

The only unknown in the equations above is $r = t/b$ which was determined experimentally.

Their experimental set-up is shown in Fig. 5. The aluminum metal foam sample (6.3 cm x 6.3 cm x 4.6 cm), is brazed at the top and bottom to two aluminum plates (4.7 mm thick), and the top plate was heated from above using patch heaters connected to a DC power supply. The surface above the heaters and the four sides were insulated using very low conductivity styrofoam. The bottom plate was cooled from below by immersing the bottom surface into a tank that contained cooling water maintained at constant temperature. Four T-type thermocouples were attached to the top and bottom plates at varying distances to measure the surface temperatures.

For different values of heat input, the temperature difference, ΔT, between the top and bottom plates was noted. The effective thermal conductivity, k_e, is then simply given by

$$k_e = \frac{L_m}{A_m(\Delta T / 2)} \quad (10)$$

A comparison of the experimental data and the analytical model revealed a value of r = 0.09 for an excellent fit. Additional data with water as the fluid validated the value of r = 0.09.

Noting that the square intersection results in a two-fold symmetry, Bhattacharya *et al*. (1999) extended the above-discussed work to include hexagonal and circular intersections that result in six-fold symmetry, see Fig. 3. Following the procedure outlined above, new analytical expressions were derived for these cases. Again, the only unknown parameter was found to be "r". Using the experimental set-up described above, they also obtained data for reticulated vitreous carbon foams. It was shown that values of r = 0.19 and 0.22, for the hexagonal and circular intersections respectively, provided an excellent fit with the experimental data. They also proposed an empirical correlation of the form given below:

$$k_{eff} = \sqrt{A[(\varepsilon k_f + (1-\varepsilon)k_s)]^2 + \frac{1-A}{\left(\frac{\varepsilon}{k_f} + \frac{1-\varepsilon}{k_s}\right)^2}} \quad (11)$$

The terms in the first set of square brackets represent the solid and fluid phases arranged in parallel (upper limit) while the second set of square brackets corresponds to the two phases arranged in series (lower limit). Equation (11) thus represents a value in between these asymptotic limits. The coefficient "A" from experimental data for the different solid-fluid

combinations was determined to be 0.38. Note that k_{fe} and k_{se} can be derived from Equations (8) and (9) by simply setting k_s and k_f to zero, respectively.

2.2 Determining K and f

Based on his experiments using loosely packed, nearly uniform-sized particles that formed a rigid and isotropic solid matrix, Darcy (1858) found that

$$\frac{dp}{dx} = \frac{\mu u}{K} \tag{12}$$

Equation (12), known as the Darcy Law, neglects fluid inertia, the effect of bounding walls and it is not known to be valid for liquids and gases at high velocities. It is now generally accepted that the pressure gradient in a rigid porous medium can be expressed as

$$-\frac{dp}{dx} = -\frac{\mu u}{K} + \frac{\rho f}{\sqrt{K}} u^2 \tag{13}$$

where K and f are related to the structure of the medium. For packed beds, a number of investigations (Scheidegger, 1974; Carman, 1939; Ergun, 1952; Macdonald *et al.,* 1979) have proposed models to establish a relationship between K, f and the structure of the medium. Such models are not generally valid for high porosity metal foams. A common and practical approach is to conduct experiments to measure pressure drop and average velocity, and use Eq. (13) to determine f and K.

Beavers *et al.* (1969) conducted experiments on high porosity media and gave value of f = 0.074. No relationship was given for K. Antohe *et al.* (1997) measured K and f for compressed metals *(ε = 0.3 - 0.7)* but did not present any correlations. Du Plessis *et al.* (1994) derived a model based on a periodic unit cell presentation, for foam samples of very small pore sizes (45 - 100 PPI) using water and glycerol as the fluid phase. For the metal foams considered in our research (5 - 40 PPI), its applicability is suspect. We, therefore, set up an experiment, Figure 6, to allow pressure drop measurements for different flow rates for the metal foams under investigation.

Noting that Eq. (13), derived from the momentum equation, assumes that the viscous drag and the convection terms are negligible, the experiment was set up to ensure fully developed flow in the test section. The metal foam samples were 6.25 cm $\times$ 4.55 cm $\times$ 19.59 cm in size and were brazed to .95 cm thick aluminum skins of size 6.25 cm $\times$ 19.59 cm. Following Vafai and Tien (1981) and Kaviany (1991), it was determined that 7.62 cm developing length would ensure fully developed flow downstream. Pressure taps at different axial locations were placed downstream of the developing length and were connected to accurate pressure transducers. An orifice plate (pipe diameter 10.16 cm, bore diameter 3.69 cm) was used to monitor the flow rate.

The pressure drop data for different axial lengths between the pressure taps, L, showed no dependence on L, indicating that the flow was fully developed. Further, for the range of velocities in the experiment, the pressure drop due to wall friction was found to be less than 0.5% of the total pressure drop. The pressure drop, therefore, could be attributed to the drag force exerted by the metal foam leading to the use of Eq. (13) for accurate determination of K and f.

Equation (13) can be written in the form

$$\frac{\Delta \rho}{L} = au + bu^2 \tag{14}$$

From a least square fit ($R^2 > 99.9\%$) of the experimental data, a and b were determined. Recalling that $a = \mu / K$ and $b = f \bullet \rho / \sqrt{K}$, both K and f were determined. The following empirical correlations fitted the K and f values accurately.

$$\frac{K}{d_p^2} = A_1 (1 - \varepsilon)^{m_1} \left(\frac{d_f}{d_p} \right)^{n_1} \tag{15}$$

$$f = A_2 (1 - \varepsilon)^{m_2} \left(\frac{d_f}{d_p} \right)^{n_2} \tag{16}$$

where $A_1 = 0.00073$, $m_1 = -0.224$, $n_1 = -1.11$, $A_2 = 0.00212$, $m_2 = -0.132$ and $n_2 = -1.63$. The choice of parameters $(1 - \varepsilon)$ and $\left(\dfrac{d_f}{d_p} \right)$ is not arbitrary. The former was included to mimic the behavior as ε approaches unity, and the latter to include the effect of fiber diameter and the pore size on the drag.

2.3 Estimating h_{sf}

No generalized correlations exist in literature for calculating the interfacial heat transfer coefficient, h_{sf}. However, noting that the radial temperature gradients are expected to be small for metal foams, heat transfer relation for flow over an isothermal external body may be deployed. The most comprehensive model for packed beds is due to Zhukauskas (1972) and is given below:

$$Nu_f = hs_f \bullet \frac{d_f}{k_f} = 0.75 \; \mathrm{Re}_d^{0.40} \; \mathrm{Pr}^{0.37} \qquad 1 \leq \mathrm{Re}_d \leq 40 \tag{17}$$

$$= 0.51 \; \mathrm{Re}_d^{0.51} \; \mathrm{Pr}^{0.37} \qquad 40 \leq \mathrm{Re}_d \leq 1000 \tag{18}$$

This correlation was derived based on a critical examination of experimental data from a variety of sources, and is strictly valid for circular cylinders only. For a metal foam, the x-section of the fibers is circular only for low porosity values. As ε increases (> 0.9), the fiber cross-section changes from being circular to almost triangular. However, an examination of the heat transfer correlations for external flow over bodies of different cross-sections (Incropera, 1997) showed that an equation of the form

$$Nu_f = C_T \; \mathrm{Re}_d^m \; \mathrm{Pr}^{0.37} \tag{19}$$

can be used for non-circular cross-sections and that exponent m varies much more slowly than constant C_T. We, therefore, decided to use Eq. (19) in our study and float C_T and determine its value by matching the numerical results with the experimental data.

2.4 Determining a_{sf}

The specific area, a_{sf}, for the metal foam structure can be calculated as (Calmidi, 1998)

$$a_{s_f} = \frac{3\pi d_f}{dp^2} \tag{20}$$

where d_f and d_p are related through equations (1) to (3).

2.5 Determining k_d

The dispersion thermal conductivity, k_d, accounts for the enhanced mixing of the fluid due to the presence of the solid phase. Dispersion in packed beds has been investigated by a number of investigators including Adnani et al. (1995), Eidsath et al. (1983), and Koch and Brady (1986). Using ensemble averaging, Koch and Brady showed that the dispersion conductivity is a function of the Peclet number and the structure of the medium. For foamed materials, Hunt and Tien (1988) have confirmed, through analysis and the supporting experiment, the linear dependence of k_d on Pe. It is noted that k_d need not be isotropic even for isotropic structures, see Adnani et al. (1995), Amiri and Vafai (1994), Gunn and DeSouza (1974) and Wakao and Kaguel (1982). In general, the streamwise and transverse dispersion conductivities, k_{dx} and k_{dy}, are additional effects to two very different transport mechanisms. In the transverse direction (y), k_{dy} has an enhancing effect over the stagnant conductivity. Hence, at high Re, considerable error can be introduced if it is not included properly. In the streamwise direction (x), k_{dx} is an additional effect on stagnant conductivity and advection. The latter is the dominant mode of transport at high Re. For the low Re encountered in our research, this effect is expected to be small. However, for accuracy, we included this effect by setting it equal to transverse dispersion, that is, $k_{dx} = k_{dy} = k_d$. An upshot of this discussion is that k_d can be written as

$$\frac{k_d}{k_e} = C_D \left(\text{Re}_K \bullet \text{Pr}_e \right) \frac{u}{u_0} \tag{21}$$

where the coefficient of thermal dispersion, C_D, is determined experimentally.

We note that Eq. (21) does not account for wall effects except through the change in velocity profile near the wall. For packed beds, Cheng and Hsu (1986), proposed the use of a wall function ℓ, that multiplies the RHS of Eq. (21) to account for reduced mixing and dispersion close to the wall, where

$$\ell = 1 - e^{-y/\beta d} \tag{22}$$

where y is the distance from the wall and d is the diameter of the particles forming the porous medium. The empirical constant β is determined from comparison with experimental data. In this postulation, the wall function is zero at the wall and exponentially reaches unity, just a few particle diameters away from the wall. For fibrous beds, the near wall variation is cubic (Koch, 1996). However, the length scaling is with respect to the Brinkman screening length (order $\sqrt{K}$) and is thus very small for metal foams. The reduced velocity at the wall should, therefore, account for the reduced dispersion close to the wall. Equation (21) is thus an appropriate model for the metal foams.

2.6 Experimental determination of K_d and C_T

The experimental set up for determining K_d and C_T is the same as shown in Fig. 6, except that now on one of the skins, 6.4 mm thick grooves, 114 mm apart, were cut in order to isolate a section of the metal foam. Patch heaters were fixed to this isolated portion of the skin between the grooves and the grooves were loosely filled with insulating material to prevent conduction losses from the heated to the unheated sections. For details, see Calmidi and Mahajan (2000). Then, two thin (2 mm) grooves were cut in the metal foam, below the grooves on the skin. This was done to prevent back-conduction of heat from the heated to the unheated sections. The isolating scheme just described achieves two purposes. First, the flow does not undergo any abrupt changes as it enters the heated section of the metal foam. Second, and more important, flow is fully developed as it enters the heated section. Six 36 gauge T-type thermocouples (axial thermocouples) were fixed along axial locations in the skin. All thermocouples were connected

to a data acquisition system and a personal computer. Flow measurement was achieved using the orifice plate. In this experiment, the average velocity, u_o, was varied from 0.6 to 3.8 m/s. For more details, see Calmidi and Mahajan (2000). The samples were chosen from a range of porosities and pore sizes, as shown in Table 1.

Table 1 Characteristics of metal foam samples used in experimental study

#	Porosity	PPI	d_f(m) fiber dia.	d_p(m) pore dia.	f	K ($*10^7$ m^2)	k_{se} (W/m-k)	k_{fe} (W/m-K)
1	0.9726	5	0.00050	0.00402	0.097	2.7	2.48	0.0256
2	0.9118	5	0.00055	0.00380	0.085	1.8	6.46	0.0237
3	0.9486	10	0.00040	0.00313	0.097	1.2	4.10	0.0248
4	0.9546	20	0.00030	0.00280	0.093	1.3	3.71	0.0250
5	0.9005	20	0.00035	0.00258	0.088	0.9	7.19	0.0233
6	0.9272	40	0.00025	0.00202	0.089	0.61	5.48	0.0242
7	0.9132	40	0.00025	0.00180	0.084	0.53	6.37	0.0237

Using the measured wall temperature data, the heat flux was converted into an average Nusselt number. The average temperature ΔT_{avg} is defined as the average of the six values of the temperature measured. That is

$$\Delta T_{avg} = \left(\sum_{i=1}^{n} T_{wi} \right) / n - T_{in} \tag{23}$$

where n is the number of points where the wall temperature was measured. It is noted that, although this value is not the actual average wall temperature, it does represent an appropriate scale to represent the temperature difference. Knowing the power input to the heaters, q,

$$Nu = h\frac{L}{k_e} = \frac{q}{A(\Delta T_{avg})} = \frac{L}{k_e} \tag{24}$$

where A is the area of cross section of the metal foam, L is the length of the heated section of the metal foam, and $k_e = k_{fe} + k_{fc}$.

The next step was to numerically solve the governing equations of transport for the conditions of the experiments and to determine C_T and k_d until the numerical simulations matched with the experimental data. To this end, the momentum and energy equations were written in non-dimensional form as follows:

$$\frac{d^2U}{dY^2} = \frac{\varepsilon}{\sqrt{Da}}(U-1) + \frac{\text{Re}_K}{Da} f \sqrt{\varepsilon}(U^2-1) \tag{25}$$

$$0 = \frac{1}{Bi_s}\left(\frac{d^2\theta_s}{dX^2} + \frac{d^2\theta_s}{dY^2} \right) - (\theta_s - \theta_f) \tag{26}$$

$$U\frac{\partial\theta_f}{\partial X} = \frac{\partial}{\partial X}\left(\left(\frac{Da}{\text{Re}_K \text{Pr}_{fe}} + C_D U \right)\frac{\partial\theta_f}{\partial X} \right) + \frac{\partial}{\partial Y}\left(\left(\frac{Da}{\text{Re}_K \text{Pr}_{fe}} + C_D U \right)\frac{\partial\theta_f}{\partial Y} \right) + \frac{Bi_f}{\text{Re}_K \text{Pr}_{fe}}(\theta_s - \theta_f)$$
$$\tag{27}$$

where

$$\text{Re}_K = \frac{u_o\sqrt{K}}{\nu}, \quad Da = \frac{\sqrt{K}}{H}, \quad Bi_s = \frac{h_{sf}\,a_{sf}\,H^2}{k_{se}}, and \ Bi_f = \frac{h_{sf}\,a_{sf}\,H\sqrt{K}}{k_{fe}} \tag{28}$$

To solve the above set of equations corresponding to the experimental conditions, a fully developed velocity profile was prescribed at the inlet. This velocity profile (function of Y alone) was calculated using the exact solution for the second-order non-linear ODE, Eq. (25). Following Vafai and Kim (1989), the exact solution due to flow through a channel is given by expressing the pressure drop in terms of the centerline velocity. It is reproduced below,

$$U = U_c\left[1 - \left(\frac{A+B}{A}\right)\left(\cosh(D(1-2Y+C))\right)^2\right] \tag{29}$$

$$A = \varepsilon f\,\text{Re}/6Da^2, \ B = \varepsilon/(4Da^2)+2A, \ C = -\frac{1}{D}a\cosh\left(\sqrt{\frac{A+B}{A}}\right)-1, \ D = \sqrt{\frac{A+B}{2}} \tag{30}$$

However, here, the average velocity u_o, and not the centerline velocity, is known. Hence the centerline velocity had to be guessed and iterated over until mass balance was achieved.

The energy equations were solved using a finite difference scheme. The ADI method of Peaceman and Rachford (Roache, 1982) was employed for this purpose. The code was validated for its accuracy by comparing the simulations with those of Yokoyama and Mahajan (1995).

First, the condition of zero dispersion (i.e., $C_D = 0$) was studied. Figure 7 shows a plot of the Nusselt number as a function of Re_KPr_e for different values of C_T with $C_D = 0$. The results are for Sample 2 in Table 1, and the experimental points are shown by the Δ symbols. As expected, the Nusselt number increases with an increase in C_T since the efficiency of heat transfer between the two phases improves. However, note that there is practically no difference in the computed results for $C_T > 0.52$ indicating that the phases are close to the thermal equilibrium condition.

With C_T fixed as 0.52, C_D was now turned on. For the metal-air samples, C_D had very marginal effect on the results indicating relatively small contribution of thermal dispersion. As a result, the simulations exhibited very little dependence on C_D. An accurate value of C_D, therefore, could not be obtained from foam-air combination. For $\text{RePr} \cong 30$, the value of k_d was only 3% of the stagnant thermal conductivity. However, when combined with the past data of Hunt and Tien (1988) for metal foams with water as the fluid, k_d was calculated to be 175% of k_e for $Re_KPr_e = 30$. The dependence on C_D was much more marked than in air and a unique value of C_D could be found to best fit the data. This value was found to be 0.06.

3. Buoyancy induced convection

Buoyancy induced convection plays an important role in cooling of electronic components. Despite significantly lower heat transfer coefficients compared to forced convection or immersion boiling, buoyancy induced convection in air is preferred for low-end applications like switching devices, consumer electronics and avionics packages due to its simplicity and reliability. Further, any increase in heat transfer rate that might be achieved through innovative designs comes at no additional penalty (unlike that of pressure drop that is experienced in forced convection). We therefore undertook an experimental and numerical research effort to evaluate the thermal performance of metal foam heat sinks[©] in buoyancy induced convection.

The experimental setup shown in Fig. 8, consisted of a large Plexiglas housing (60.96 cm x 60.96 cm x 40.64 cm) which stationed the metal foam sample. Holes were drilled on the base of the samples to insert Firerod[®] cartridge heaters (see Fig. 9). The base of the sample was insulated using low conductivity Styrofoam insulation. The cartridge heaters were powered by a DC power

supply. The base and ambient temperatures were monitored using 0.127 mm (36 AWG) T-type thermocouples connected to an Omega DASTC data acquisition system.

Experiments were conducted on foam samples of different porosities and pore densities. For each pore density corresponding to 5, 10, 20 and 40 PPI, two samples of different porosities were chosen (see Table 2). During a typical experimental run, the power to the heaters was varied to achieve different base plate temperatures and hence Rayleigh numbers.

Table 2 Experimental metal foam samples

PPI	Porosity	Permeability (x 10^7) [m^2]
5	0.899	1.99
	0.93	2.07
10	0.9085	1.08
	0.9386	1.17
20	0.92	1.06
	0.9353	1.17
40	0.9091	0.507
	0.9586	0.599

For the parameters listed in Table 2, a plot of $Nu = \dfrac{hL^*}{k_f}$ against $Ra = \dfrac{g\beta\Delta T L^{*3}}{\alpha v}$ is shown in Fig. 10, where $L^* = 4A_c/b$ The following conclusions can be drawn from these plots.

For a given porosity, the resistance to flow decreases with increase in pore size. The result is enhanced flow and heat transfer rate. For a given PPI (pore density), the performance gets enhanced with decrease in porosity. This indicates that conduction is still the dominant mode of heat transfer. This result is consistent with the previous results on forced convection in metal foams, Calmidi and Mahajan (2000).

Using least squares fit, the best correlation obtained was

$Nu = 13.24\, Ra^{0.25}\, Da^{0.17}$ (31)

with a maximum error of $\pm$ 7%. The choice of the index for Ra was based on the existing correlations for buoyancy induced convection on a horizontal flat plate. Note that the porosity dependence is captured through the Darcy number, which is a function of the permeability K and hence porosity of the medium.

A detailed numerical analysis was also carried out for flow induced in high porosity metal foams heated from below. The governing equations are those listed in Section 2 except that buoyancy terms, $\rho_f\mathbf{g}$, $g\beta\left(\langle T_f \rangle^f - T_\infty\right)$ are added to the momentum equation (5).

As before, the effects of thermal dispersion were investigated. The conditions under which the local thermal equilibrium assumption may not be valid were identified. Control volume based, semi-implicit method (Patankar, 1980) was used to solve the governing set of equations and the boundary conditions. For complete details, see the two companion papers by Phanikumar and Mahajan (2000) presented at this conference. Steam function and isotherm plots were given to provide an insight into the flow and thermal fields. A value of $C_T = 0.51$ was determined to provide a good match between the computational results and the experimental data. With the

value of C_T determined, a parametric study was conducted for different values of Darcy number. Figure 11 shows their results. Experimental data for aluminum metal foam samples is also plotted. A good agreement is seen. It was also shown that departure from the assumption of local thermal equilibrium increases at higher Rayleigh and Darcy numbers. For complete details, the reader is referred to the two papers cited above.

4. Pool Boiling in FC-72

Motivated by our desire to fully explore the potential of metal foams for high thermal dissipation, we also undertook an experimental investigation of pool boiling of a Flourinert fluid, FC-72, in highly porous metal foam heat sinks.

A picture of the metal foam sample used in our boiling experiments is shown in Fig. 9. Samples with porosities from 89.9% to 98.08% and pore distribution between 5 PPI and 40 PPI were used. High flux (220 kW/m^2) Firerod$^®$ cartridge heaters were inserted in the aluminum block and used as heat sources.

A schematic of the complete experimental apparatus is shown in Fig. 12. The metal foam was fitted on to the square cavity in the center of an Ultem$^®$ base plate. The base plate was mounted on a cylindrical Plexiglas casing that houses the fiberglass and styrofoam insulation required to minimize conductive heat losses through the base. The heat sink was housed in a rectangular polycarbonate container enclosed by an outer Plexiglas cylindrical container. This enclosure provided an insulating air layer that reduced convective heat losses from the sides of the polycarbonate container. A nichrome wire coil wrapped around the polycarbonate container was heated with a PID controlled power supply to maintain its surface temperature at that of the bulk temperature of the saturated fluid. This minimized the steady state conductive heat losses from the boiling fluid across the container. Recirculating water from a chiller was fed to the aluminum condensing coils and a distillation flask was used to ensure that no uncondensed vapors left the system. The valve connecting the boiling chamber and the distillation unit condenser was left open at all times to balance the chamber pressure with the atmosphere. The setup was made leak proof by bolting the enclosure to the base plate and applying proper sealant. For complete details, see Arbelaez *et al.* (2000).

The pool boiling data for the 10 PPI and 20 PPI samples are presented in Fig. 13. It is noted from Fig. 13 that in the natural convection regime, there is a significant improvement (2-4 times) in heat transfer compared to that for the flat plate. In the presence of metal foam, conduction plays a major role along with natural convection. The aluminum foam placed on the heated surface acts liked finned extensions removing heat from it by conduction. Also, the flow of the rising fluid is disturbed by the complex metal foam matrix that further enhances the heat transfer rate from the metal foam strands to the ambient fluid. The net result, as seen in Fig. 13 is a marked increase in the heat transfer value.

Incipient boiling commences at a superheat of 8 to 10°C. This is slightly lower than that observed for the flat plate. Also, the temperature excursion associated with transition from natural convection to nucleate boiling is not observed. Earlier incipience and the absence of significant hysteresis suggest that the intricate metal foam structure helps sustain potentially active cavities required for nucleation, even in the presence of a highly wetting medium. Two of the high porosity samples tested (5 PPI, 97.08% and 10 PPI, 98.08%), however, do exhibit a small temperature excursion of 2°C at incipience. The slight anomaly is possibly due to less effective vapor trapping in the nucleation cavities by the relatively larger pores encountered in the low PPI and high porosity metal foams. The boiling data obtained in the low heat flux regime

is qualitatively similar to the sand blasted and vapor blasted surfaces tested by Anderson and Mudawar (1989]) where an earlier incipience, promoted by the roughened surfaces, was reported at superheats of 13.1^{o}C and 9.2^{o}C respectively.

Similar to the observations in the natural convection regime, nucleate boiling is significantly enhanced in the presence of metal foams. The predominant mode of heat transfer in this regime rapidly changes, with increasing heat flux, from natural convection and conduction to that of heat removed from the surface by the departing bubbles and the local agitation produced by the liquid flowing in behind the wake of the departing bubbles. The high conductivity of aluminum results in a portion of the metal foam above the heated surface taking part in the bubble generation process. This causes a marked increase in the boiling surface area and hence the total number of active nucleation sites present as compared to that of the flat plate. With increasing heat flux there is a further increase in this region of the metal foam participating in active boiling. Also, the open foam structure provides a very tortuous path for the rising bubbles producing thereby intensive agitation behind their wake. The result is further enhancement in heat transfer.

It is also noted that in the high flux nucleate boiling regime the slope of the boiling curve decreases with increasing heat flux. The number of bubble nuclei present in the porous matrix is mostly limited by the number of cavities and does not increase dramatically with an increase in heat flux. Vapor slugs released from the heated surface and the metal foam fibers begin to coalesce, forming vapor envelopes over the metal foam fibers. This retards the removal of vapor from the heated surface and hence restricts heat transfer. However, owing to the high conductivity of the aluminum foam, while film formation starts taking place near the heated surface; regions further away from the base still witness active nucleate boiling. The effect of this is to smoothen out the transition to film boiling. A similar effect was observed by Afgan *et al*. (1985). Though the porous medium used was structurally different from the metal foams, they observed bubble boiling along with the formation of a stable vapor film at the base of the porous layer before the critical heat flux limit was reached. The gradual transition to film boiling is also evidenced by the fact that this region exists over a larger superheat value as compared to observations made by Marto and Lepere (1982) and Anderson and Mudawar (1989). The transition to film boiling is still marked by a sudden increase in the surface temperature, though the temperature jump noted is as small as 50°C. This is much less than that reported by Mahajan (1979) for boiling of the Fluorinert FC-70, which has similar properties to FC-72, over a platinum wire.

The delay in transition to film boiling is accompanied by an increase in the heat flux value at which it takes place. Hence, a significant increment in the critical heat flux (CHF) value compared to that of the flat plate is observed. A CHF value as high as 288 kW/m^2 was reported for the 20 PPI, 92.01% sample. This is approximately 50% higher than the CHF value observed in the flat plate case. The values are also higher than those reported by Marto and Lepere (1982) for boiling in FC-72 over three commercially available enhanced copper surfaces. Although comparable to the results obtained by Anderson and Mudawar (1989) for the microfin and microstud and the microgrooved surfaces, the enhancement is significant compared to the vapor and sand blasted surfaces and the surface with artificial cavities.

The boiling curves at different porosities for the 40 PPI samples are plotted in Fig. 14, respectively. The figures indicate a dependence of heat transfer on the porosity of the metal foam. For the same superheat, it is found that the heat transfer rate is higher at lower porosities and is possibly due to the higher effective thermal conductivity of the lower porosity metal foam sample. Also, the increase in the heat transfer rate suggests the presence of larger number of

active nucleation cavities in the lower porosity samples. A comparison of the boiling curves for the different PPI samples at similar porosities (93.5%-94%) is shown in Fig. 15. A clear trend observed with an increase in PPI is an enhancement in the heat transfer performance in both the natural convection and nucleate boiling regimes. This is again attributed to the higher effective boiling surface area and the larger hydrodynamic disturbances associated with the higher PPI sample.

Based on the collected experimental data, the following correlation was proposed between the Nusselt number, Stefan number and Bond number.

$$Nu = \frac{h d_p}{k_{eff}} = 1.497 \, S^{.512} \, Bo^{0.384} \tag{32}$$

The Nu values obtained from the experiment are also shown against the values obtained with the correlation. The equation correlates most of the experimental data satisfactorily within ± 40%, see Fig. 16.

5. Concluding Remarks

High porosity metal foams (e > 0.90) are attractive candidates for many thermal engineering applications including thermal management of electronic systems and compact heat exchangers. However, the transport phenomena associated with these materials are complex and need to be thoroughly understood before their potential can be realized. Many of the existing correlations and formulations at lower and medium porosities do not apply at very high porosities . In this paper, our research work on this topic has been presented. The combined analytical and experimental work has created a knowledge base on effective thermal conductivity, convective coefficient including thermal dispersion and pressure drop. It has been shown that higher heat transfer coefficients are achieved in forced convection, buoyancy induced convection and pool boiling. Further improvements are possible with optimization of foam geometry.

It has also been shown recently that finned metal foams that combine conventional longitudinal finned heat sinks and metal foams offer even higher heat transfer rates than metal foams also. Some initial work on selectively compressing the foams along one of the axes of orientation indicates promise for preferred directional heat transfer. These present opportunities for further research.

6. References

Adnani, P., Catton, I., and Abdou, M. A. 1995, "Non-Darcean Forced Convection in Porous Media with Anisotropic Dispersion", *ASME J. Heat Transfer*, 117, 447-451.

Afgan, Naim H., and Jovic, L. A., and Kovalev, S. A., and Lenykov, V.A., (1985), "Boiling Heat Transfer from Surfaces with Porous Layers", *Int. J. Heat Mass Transfer*, 28, 415-422

Anderson, T.M, and Mudawar, I., 1989, "Microelectronic Cooling by Enhanced Pool Boiling of a Dielectric Fluorocarbon Liquid", *ASME Journal of Heat Transfer*, 111, 752-759.

Arbelaez, F., Sett, S., and Mahajan, R. L. 2000, "An experimental study on pool boiling of saturated FC-72 in highly porous aluminum metal foams", accepted for presentation and

proceedings publication, the 34th National Heat Transfer Conference, Pittsburgh PA, Aug. 20-22.

Amiri, A and K. Vafai, 1994, "Analysis of Dispersion Effects and Non-Thermal Equilibrium, Non-Darcian, Variable porosity Incompressible Flow Through Porous Media", *Int. J. Heat Mass Transfer,* vol. 37, No. 6, pp. 939-954.

Amiri, A., Vafai, K., and Kuzay, T. M., 1995, "Effects of Boundary Conditions on Non-Darcian Heat Transfer Through Porous Media and Experimental Comparisons", *Numerical Heat Transfer*, Part A, 27, pp. 651-664.

Antohe, B. V., Lage, J. L., Price, D. C. and Weber, R. M. 1997, "Experimental determination of permeability and inertia coefficients of mechanically compressed aluminum porous matrices", *ASME J. Fluids Eng.*, 119, no. 2, 404.

Bear, J., (1972), Dynamics of Fluids in Porous Media, pp. 125-127.

Beavers, G. S., and Sparrow, E. M., 1969, "Non-Darcy Flow through Fibrous Porous Media", *ASME J. Applied Mechanics*, 36, no. 4, 711-714.

Bhattacharya, A., Calmidi, V. V. and Mahajan, R. L., 1999, "An analytical-experimental study of the determination of the effective thermal conductivity of high porosity fibrous foams", ASME International Mechanical Engineering Congress and Exposition, AMD vol. 233, 13-20.

Brinkman, H.C., 1947, "A Calculation of the Viscous Force Exerted by a Flowing Fluid on a Dense Swarm of Particles", *Appl. Sci. Res*., 27-34.

Calmidi, V. V. 1998, "Transport phenomena in high porosity fibrous metal foams", Ph.D. Thesis, University of Colorado, Boulder, CO USA.

Calmidi, V.V. and Mahajan, R.L., 1999, "The effective thermal conductivity of high porosity metal foams", *ASME Journal of Heat Transfer*, 121, 466-471.

Calmidi, V. V. and Mahajan, R. L. 2000, "Forced convection in high porosity metal foams", to appear in ASME J. Heat Transfer.

Carman, P.C., 1939, "The Determination of Specific Surface Area of Powder I", *J. Soc. Chem. Ind.*, 57, pp. 225-234.

Cheng, P. and Hsu, C. T., 1986, "Applications of Van Driest's mixing length theory to transverse thermal dispersion in forced convective flow through a packed bed", *Int. Commun. Heat Mass Transfer*, 13, 613-625.

Darcy, H., 1856, "Les Fontaines Publiques de la ville de Dijon", Dalmont, Paris.

Du Plessis, P., Montillet, A., Comiti, J., and Legrand, J., 1994, "Pressure Drop Prediction for Flow through High Porosity Metallic Foams", *Chem. Engg. Sci.*, 49, 3545-3553.

Eidsath, A., Carbonell, R. G., Whitaker, S., and Herrmann, L. R., 1983, "Dispersion in pulsed systems-III, comparison between theory and experiments in paced beds", *Chem. Engng. Sci*., 38, 1803-1816.

Ergun, S., 1952, "Fluid Flow through Packed Column", *Chemical Engineering Progress,* 48, No. 2, pp. 89-94.

Gunn, D. J. and DeSouza, J.F.C., 1974, "Heat transfer and axial dispersion in packed beds", *Chem. Engng. Sci.*, 29, 1363-1371.

Hunt, M. L., and Tien, C. L., 1988,"Effects of Thermal Dispersion on Forced Convection in Fibrous Media", *Int. J. Heat Mass Transfer*, 31, 301-309.

Incropera, F.P., 1997, *Introduction to Heat Transfer*, John Wiley & Sons, New York .

Jiang, P.-X., Ren, Z.-P. and B.-X. Wang 1999, "Numerical Simulation of Forced Convection Heat Transfer in Porous Plate Channels Using Thermal Equilibrium and Nonthermal Equilibrium Models", *Numerical Heat Transfer – Part A*, vol. 35, 99-113.

Kaviany, M., 1991, Principles of Heat Transfer in Porous Media, Springer-Verlag, New York.

Kececioglu, I., and Jiang, Y., (1994), "Flow through Porous Media of packed Spheres Saturated with Water", *ASME Journal of Fluids Engineering*, 116, 164-170.

Koch, D. L. 1996, "Hydrodynamic diffusion near solid boundaries with applications to heat and mass transport into sheared suspensions and fixed-fibre beds", *J. Fluid Mech.*, 318, 31-47.

Koch, D. L. and Brady, J. F. 1986, "The effective diffusivity of fibrous media", *AIChE J.*, 32, 575-591.

Lee, Y. C., Zhang, W., Xie, H. and Mahajan, R. L. 1993, "Cooling of a FCHIP package with 100 W, 1 cm^2 chip", *Proceedings of the 1993 ASME Int. Elect. Packaging Conference*, 1, 419-423.

Macdonald, I. F., El-Sayed, M.S., Mow, K., and Dullien, F. A. L., (1979), "Flow through Porous Media: The Ergun Equation Revisited", *Industrial chemistry Fundamentals*, 18, 199-208.

Mahajan, R.L., 1979, "Determination and Control of Heater Surface Temperature in Condensation Soldering", *Proceedings of the Technical Program NEPCON*, West Anaheim CA.

Marto, P.J., and Lepere, Lt. V.J., 1982, "Pool Boiling Heat Transfer from Enhanced Surfaces to Dielectric Fluids", *ASME Journal of Heat Transfer*, 104, 292-299.

Nield, D.A. and Kuznetsov, A.V. 1999, "Local Thermal Nonequilibrium Effects in Forced Convection in a Porous Medium Channel", *Int. J. Heat Mass Transfer*, 42, 3245-3252.

Patankar, S.V. (1980), *Numerical Heat Transfer and Fluid Flow*, Hemisphere, Washington, D.C.

Phanikumar, M. S. and Mahajan, R. L. 2000, "Non-Darcy convection in a high porosity medium heated from below: effects of thermal dispersion and local thermal non-equilibrium - Part 1. Problem formulation", Proceedings ENCIT 2000, Brazilian Congress of Thermal Engineering and Science, October 2-5, Porto-Allegre, Brazil.

Phanikumar, M. S. and Mahajan, R. L. 2000, "Non-Darcy convection in a high porosity medium heated from below: effects of thermal dispersion and local thermal non-equilibrium - Part II. Numerical and experimental results", Proceedings ENCIT 2000, Brazilian Congress of Thermal Engineering and Science, October 2-5, Porto-Allegre, Brazil.

Roache, P. J., 1982, *Computational Fluid Dynamics*, Hermosa, Albuquerque, New Mexico.

Scheidegger, A.E., 1974, The Physics of Flow through Porous Media, University of Toronto Press, Toronto.

Vafai, K. and Kim, S. J. 1989, "Forced convection in a channel filled with a porous medium: An exact solution", *ASME J. Heat Transfer*, 111, 4, 1103-1106.

Vafai, K., and Tien, C. L., 1981, "Boundary and Inertia Effects on Flow and Heat Transfer in Porous Media", *Int. J. Heat Mass Transfer*, 24, 195-203.

Wakao, N. and Kaguei, S. 1982, *Heat and Mass Transfer in Packed Beds*, Gordon and Breach, New York.

Whitaker, S. 1967, "Diffusion and dispersion in porous media", *A. I. ChE. J.*, 13, 420-427.

Wooding, R. A., (1963), "Convection in a Saturated Porous Medium at larger Reynolds number or Peclet number", *J. of Fluid Mechanics*, 15, 527-544.

Yokoyama, Y. and Mahajan, R. L. 1995, "Non-Darcian convective heat transfer in a horizontal duct", *ASME Publications*, HTD-309, 83-92.

Zhukauskas, A., 1972, "Heat transfer from tubes in cross flow", in *Adv. Heat Transfer*, vol. 8, Academic Press, New York.
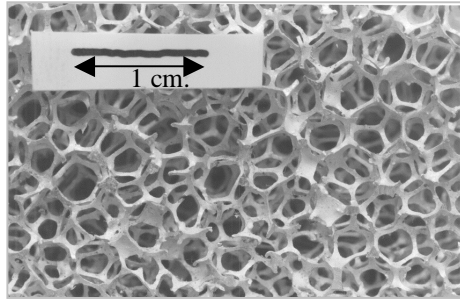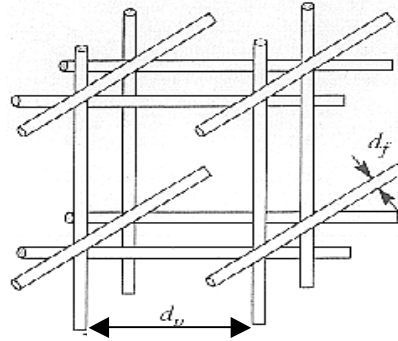
FIGURES

Figure 1: Magnified view of metal foam

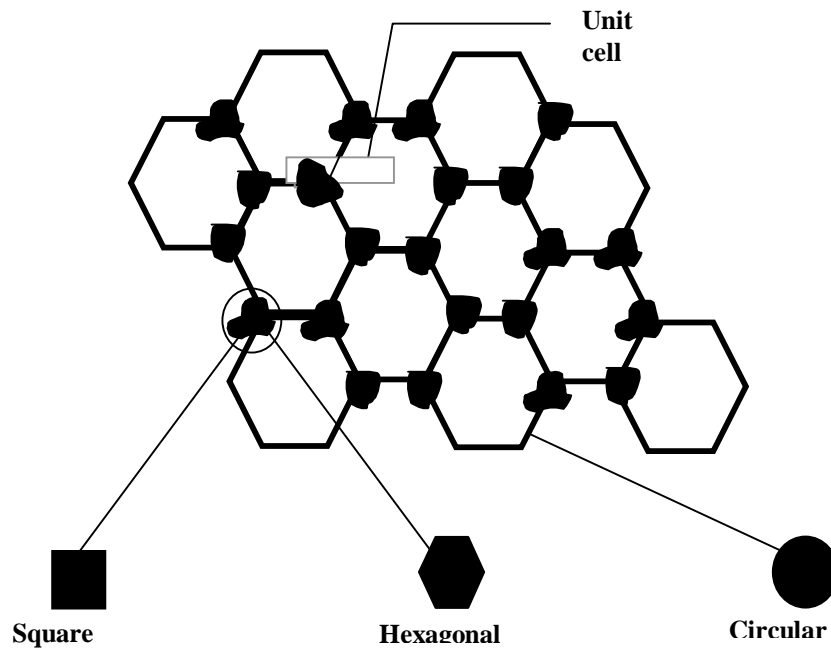**Figure 2: Open-cell representation of metal foam structure**

Figure 3:Analytical model showing the three different intersection shapes used
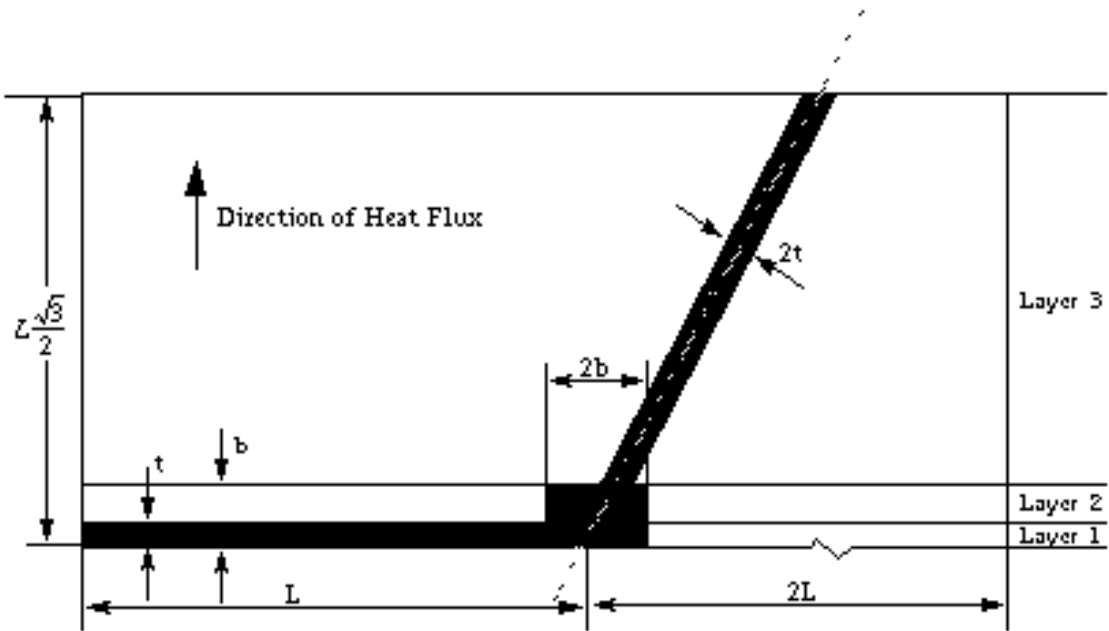
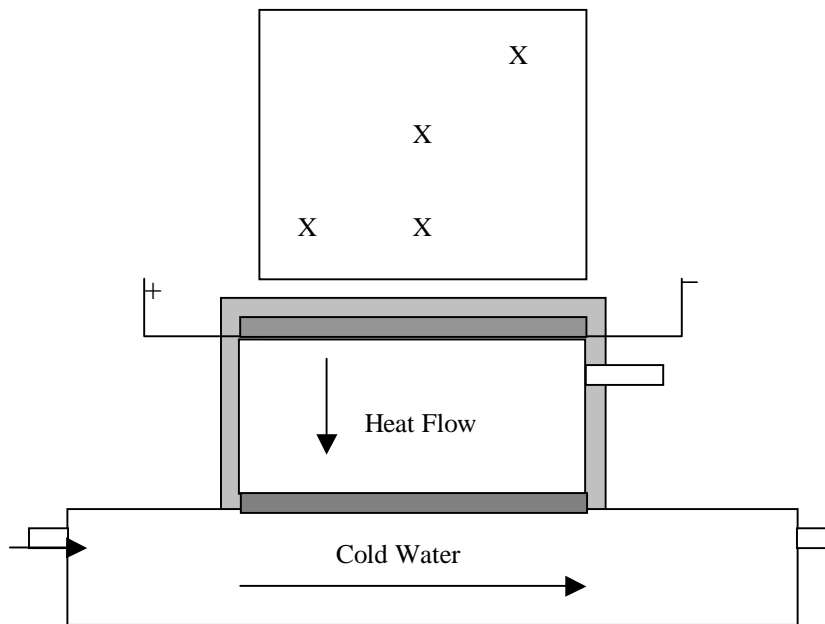**Figure 4: Unit cell for the square intersection of Calmidi and Mahajan (1999)**

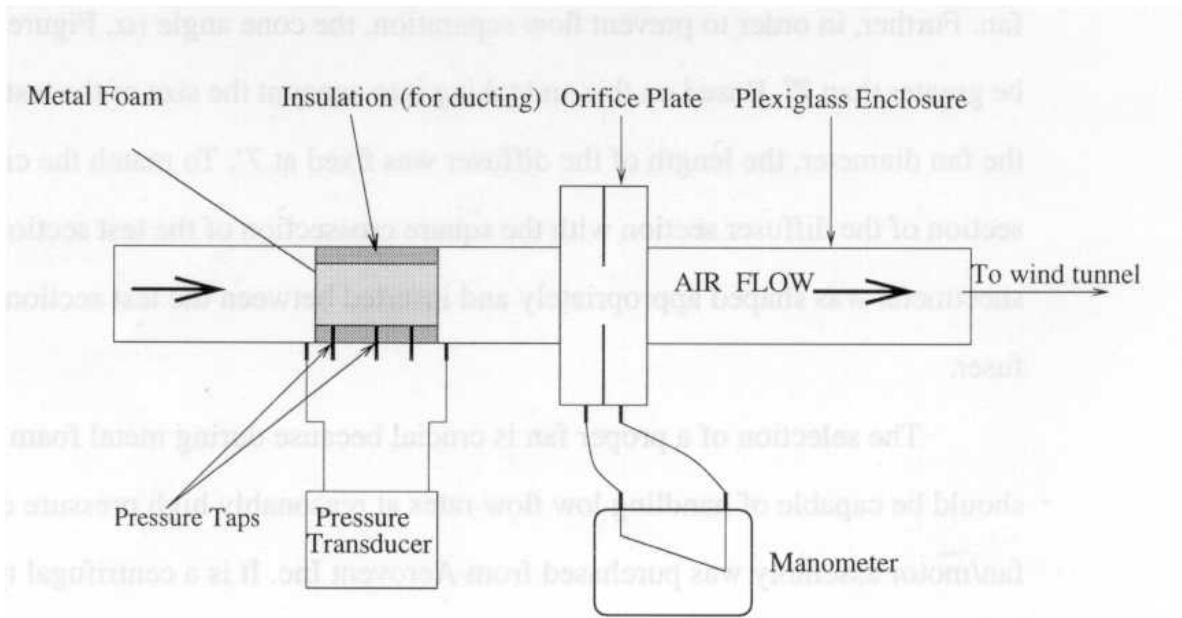**Figure 5: Schematic of the experimental set-up and thermocouple positions**

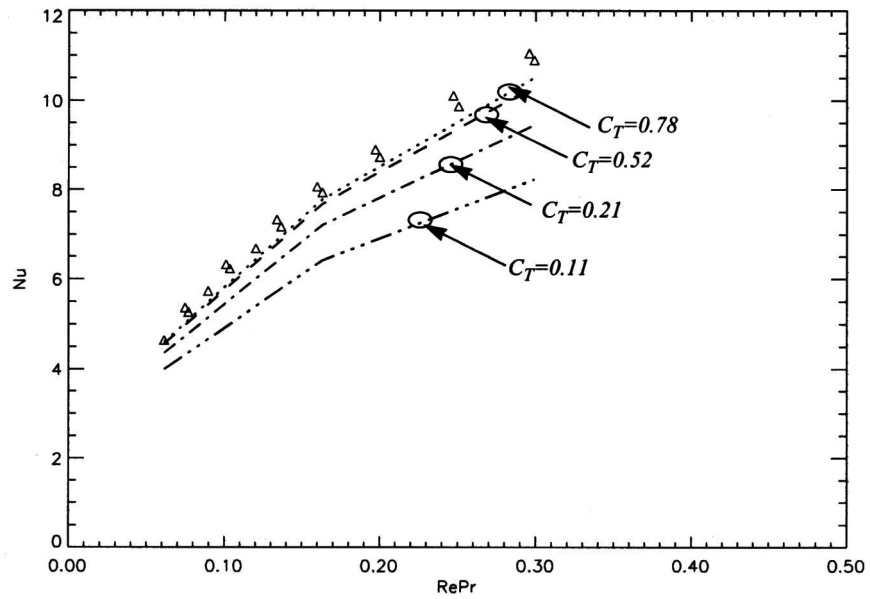**Figure 6: Schematic of the experimental set-up used for pressure drop measurements**

Figure 7: *Nu* as a function of *$Re_k Pr_e$* for different values of *C_T*
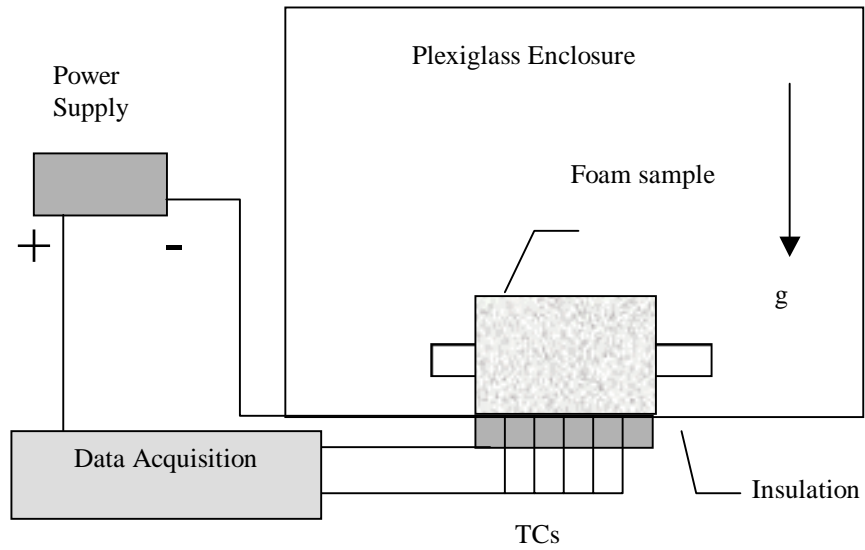
Figure 8: Schematic diagram of the experimental set-up for buoyancy induced convection
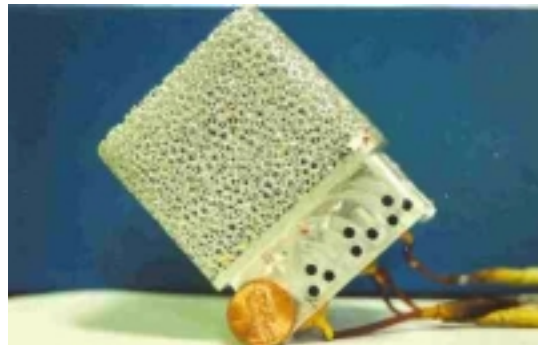
Figure 9: Picture of a typical sample used in our experiments
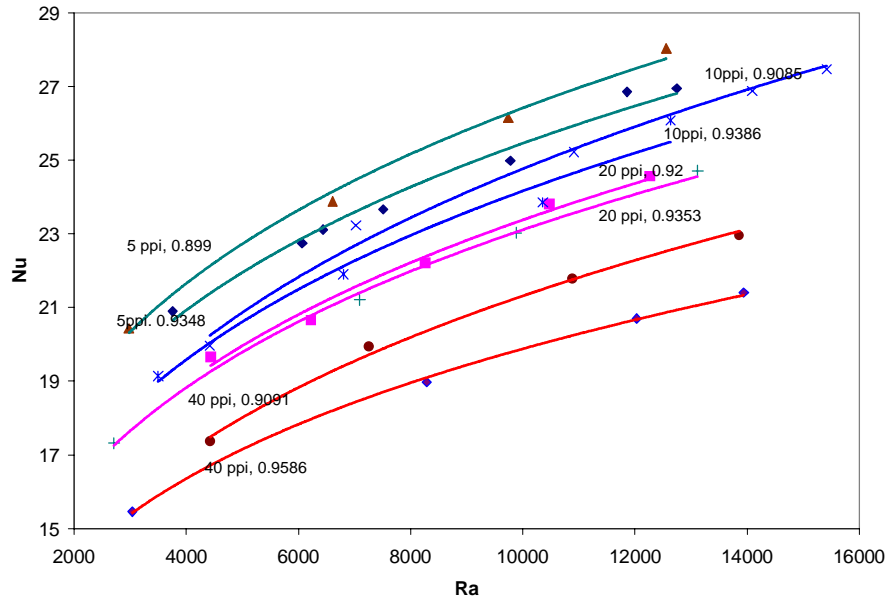
Figure 10: Heat transfer in metal foams heated from below: symbols, experimental data; lines, empirical correlation (Eq. 31).
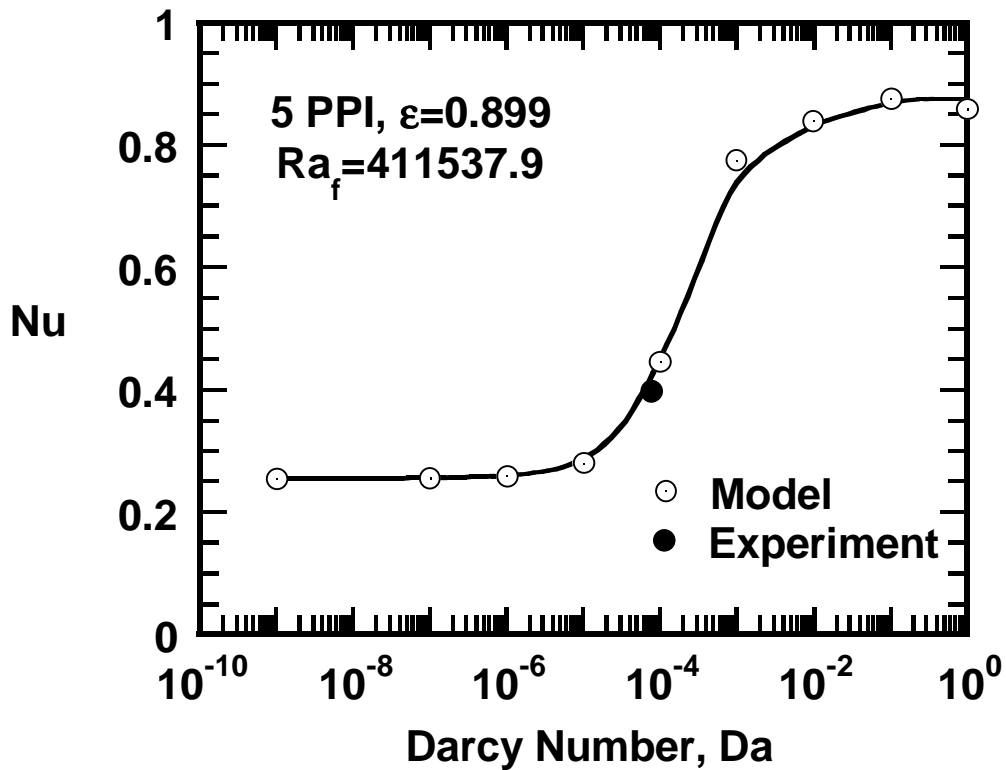
Figure 11. Effect of Darcy number on heat transfer for aluminum – air
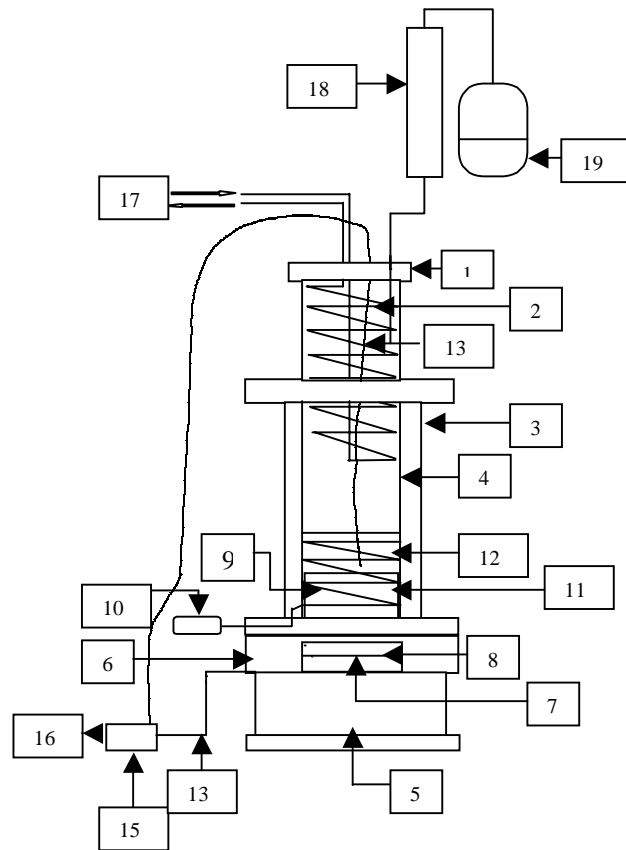
4. Polycarbonate Lid	10. PID Controller
5. Condenser Coils	1. Aluminum Foam
6. Plexiglass Outer Container	2. FC-72

7. Polycarbonate Inner Container	3. Thermocouples
	  a) In FC-72
	  b) In Metal Foam

8. Fiber Glass & Styrofoam Insulation	15. DAQ Board
9. Ultem® Base Plate	16. PC
10. DC Power	17. Chiller
11. Cartridge Heaters	18. Distillation Unit
	19. Coolant

Figure 12 Apparatus for pool boiling
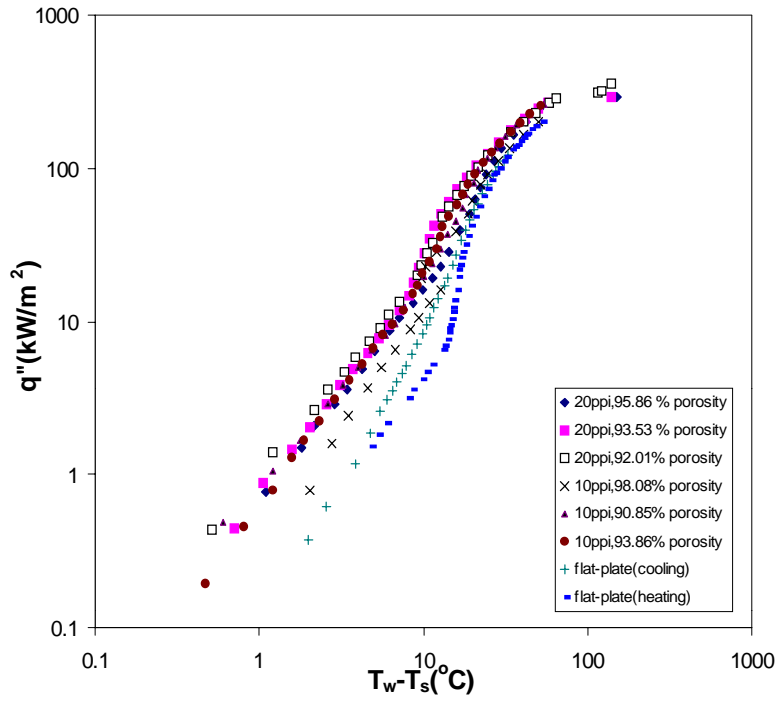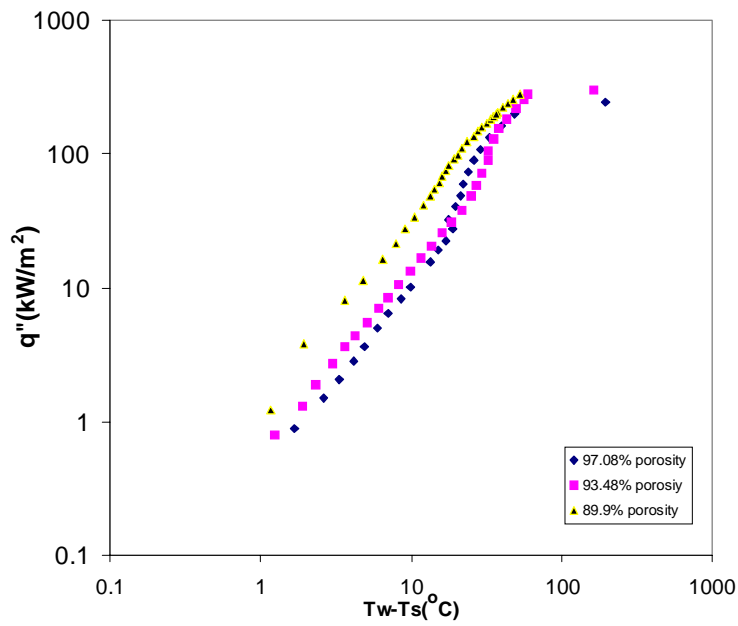
Figure 13. Boiling in porous media

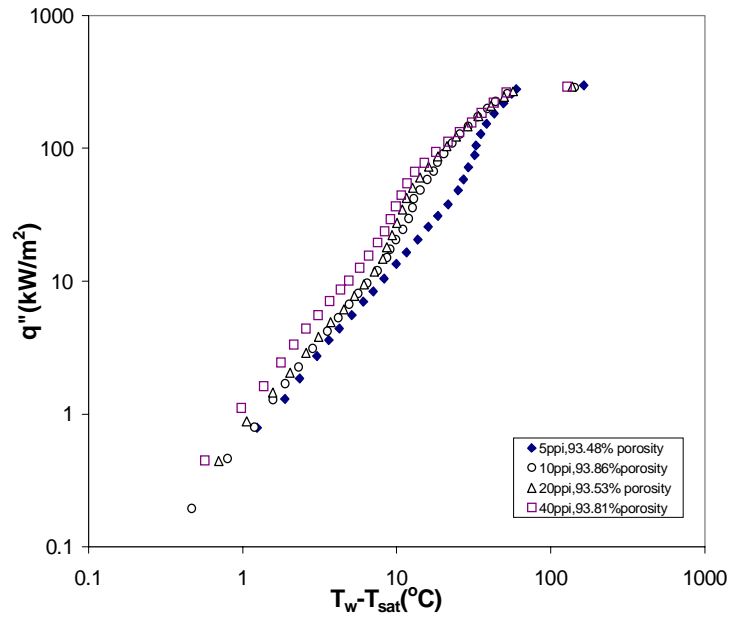**Figure 14 Boiling Curves for 5PPI at different porosities**
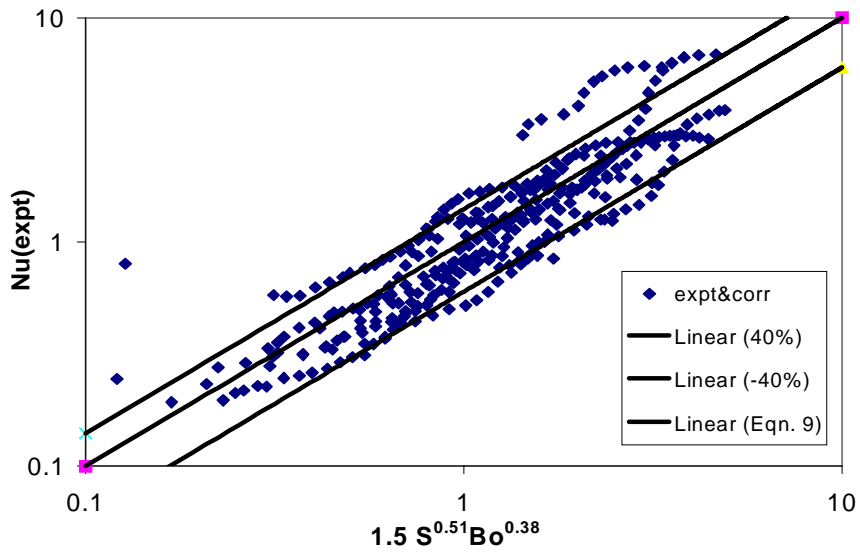
Figure 15 Effect of PPI on Heat Transfer

Figure 16 Heat Transfer Performance Correlation